AJNR

Diffusion Analysis of Intracranial and Head and Neck Epidermoid and Temporal Bone Cholesteatoma

Fabrício Guimarães Gonçalves, Amirreza Manteghinejad, Zekordavar Rimba, Dmitry Khrichenko, Angela N Viaene and Arastoo Vossough

AJNR Am J Neuroradiol published online 12 June 2024
http://www.ajnr.org/content/early/2024/06/12/ajnr.A8376

Published June 12, 2024 as 10.3174/ajnr.A8376

ORIGINAL RESEARCH

Diffusion Analysis of Intracranial and Head and Neck Epidermoid and Temporal Bone Cholesteatoma

Fabrício Guimarães Gonçalves[¥], Amirreza Manteghinejad[¥], Zekordavar Rimba, Dmitry Khrichenko, Angela N Viaene, Arastoo Vossough

ABSTRACT

BACKGROUND AND PURPOSE: Intracranial epidermoid tumors (IET), temporal bone cholesteatomas (TBC), and head and neck epidermoid cysts (ECs) are typically slow-growing, benign conditions arising from ectodermal tissue. They exhibit increased signal on diffusion-weighted imaging (DWI). While much of the imaging literature describes these lesions as showing diffusion restriction, we aimed to investigate these qualitative signal intensities and interpretations of restricted diffusion with respect to normal brain structures. This study aims to quantitatively evaluate the apparent diffusion coefficient (ADC) values and histogram features of these lesions.

MATERIALS AND METHODS: This retrospective study included children with histologically confirmed IET, TBC, or EC diagnoses. Lesions were segmented, and voxel-wise calculation of ADC values was performed along with histogram analysis. ADC calculations were validated with a second analysis software to ensure accuracy. Normal brain regions of interest—including the cerebellum, white matter, and thalamus—served as normal comparators. Correlational analysis and Bland-Altman plots assessed agreement between software for ADC calculations. Differences in the distribution of values between the lesions and normal brain tissues were assessed using Wilcoxon rank sum and Kruskal-Wallis tests.

RESULTS: Forty-eight pathology-proven cases were included in this study. Among them, 13(27.1%) patients had IET, 14(29.2%) had EC, and 21(43.7%) had TBC. The mean age was 8.67±5.30, and 27(52.9%) were female. The intraclass correlation for absolute agreement for lesional ADC between the two software was 0.997(95%CI=0.995-0.998). The IET, EC, and TBC median ADC values were not significantly different (973.7vs.875.7vs.933.2 x10-6 mm2/s, p=0.265). However, the ADCs of the three types of lesions were higher than those of three normal brain tissue types (933vs.766, x10-6 mm2/s, p<0.0001).

CONCLUSIONS: The ADC values of IET, TBC, and EC are higher than those of normal brain regions. It is not accurate to simply classify these lesions as exhibiting restricted diffusion or reduced diffusivity without considering the tissue used for comparison. The observed hyperintensity on DWI compared to the brain is likely attributable a relative higher contribution of T2 shine-through effect.

ABBREVIATIONS: TBC= Temporal Bone Cholesteatomas; IE= Intracranial Epidermoid; EC= Head and Neck Epidermal Inclusion cysts; DWI= Diffusion-Weighted Imaging; ADC= Apparent Diffusion Coefficient.

Received 01-Mar-2024; accepted after revision 04-Jun-2024.
From the Department of Radiology (F.G.G.), Children's of Alabama, Birmingham, AL, USA; Department of Radiology (A.M., Z.R., D.K), Children's Hospital of Philadelphia, Philadelphia, PA, USA; Department of Radiology (A.V.), Department of Pathology and Laboratory Medicine (A.N.V.), Children's Hospital of Philadelphia, Perelman School of Medicine, University of Pennsylvania, Philadelphia, PA, USA

¥ = Indicates co-first authors

The authors declare no conflicts of interest related to the content of this article.

Please address correspondence to Amirreza Manteghinejad, MD, Department of Radiology, Children's Hospital of Philadelphia, 3401 Civic Center Blvd., Philadelphia, PA 19104, USA; e-mail: manteghina@chop.edu.

SUMMARY SECTION

PREVIOUS LITERATURE: Despite some quantitative studies of the ADC values of IEs, TBCs, and ECs, significant portions of the imaging literature and teachings still describe these lesions as having diffusion restriction without explicitly mentioning a comparator.

KEY FINDINGS: The ADCs of IEs, TBCs, and ECs were higher than three representative normal brain tissue types, including thalamus, cerebellum, and white matter.

KNOWLEDGE ADVANCEMENT: IEs, TBCs, and ECs do not have restricted diffusion or reduced diffusivity compared to the brain. This knowledge will help in use of quantitative diffusion measures for imaging interpretation and diagnosis of these lesions. The observed DWI hyperintensity is likely more attributable to relatively higher contribution of T2 shine-through effect.

Copyright 2024 by American Society of Neuroradiology.

INTRODUCTION

Intracranial epidermoid (IE), temporal bone cholesteatomas (TBC), and head and neck epidermal inclusion cysts (EC) are typically slow-growing lesions arising from ectodermal tissue[1–3]. These benign entities are characterized by specific locations and distinctive features on computed tomography (CT) and magnetic resonance imaging (MRI)[4–6]. Despite their differences, these lesions commonly exhibit increased signal intensity on trace diffusion-weighted images (DWI)[7].

Increased DWI signal can result from both restricted (reduced) diffusion and T2 shine-through effect[8]. Diffusion restriction occurs when there is a decrease in molecular diffusion due to reduced free space for movement. On MRI, restricted diffusion is indicated by increased DWI signal intensity and reduced apparent diffusion coefficient (ADC) values[9].

The 'T2 shine-through' effect increases when an elevated signal intensity on DWI is not predominantly due to restriction of water diffusion but instead largely results from an inherently high T2 signal in the tissue[10]. This phenomenon can lead to the misinterpretation of hyperintense DWI signal as indicative of diffusion restriction when it is not. Commonly observed in tissues with prolonged T2 relaxation times, such as in subacute infarctions and vasogenic edema, the T2 shine-through effect is also manifested in various other pathological conditions[11].

In 1990, Tsuruda et al. first demonstrated the use of DWI in diagnosing IEs[12]. They assessed the ADC values of two IEs that were confirmed through surgery, finding that their ADC values were comparable to those of normal brain parenchyma, which is not in keeping with diffusion restriction[12]. This was followed by additional authors comparing the values with CSF[13–16]. In 2002, Fitzek et al. first demonstrated that ADC of TBCs was in the range of brain values[17]. In three patients in whom ADC could be calculated, the ADC was in the range of brain values (subcortical white matter and gray matter. Despite these findings, a considerable portion of subsequent imaging literature has depicted IEs, TBCs, and ECs as exhibiting diffusion restriction without explicit mention of comparators[6,18–22]. We have also personally seen comparisons of the diffusivity of some of these lesions to the brain in various practices within and outside the United States or during national or international conference lectures.

This study used quantitative ADC measurements to determine whether the DWI hyperintense signal detected in these specific ectodermal-origin masses is due to restricted diffusion. We assess whether pediatric IEs, TBCs, and ECs exhibit diffusion restriction compared to adjacent structures. Consequently, the primary objective of this study is to quantify ADC distribution histograms in IEs, TBCs, and ECs in pediatric subjects.

MATERIALS AND METHODS

Study design and inclusion criteria

This study is a retrospective, cross-sectional analysis conducted at a large academic children's hospital. The hospital Institutional Review Board reviewed and approved the study. Due to its retrospective nature, a waiver for documentation of informed consent was granted. Inclusion criteria were an age at diagnosis under 18 years, the availability of preoperative MRI, and a histologically confirmed diagnosis of IE, TBC, and ECs. Data were retrieved by searching our pathology and radiology databases (mPower by Nuance Communications Inc., Burlington, MA; and Illuminate InSight, Overland Park, KS) for cases of IE, TBC, and head and neck ECs. Demographic data were obtained from our electronic medical records system (Epic Systems Corp., Verona, WI). Following data extraction, all records were merged using the Medical Record Number. Exclusion criteria included patients whose lesions were not within the intracranial compartment or the head and neck region, those without available preoperative MRI scans, and cases where the diffusion MRI series lacked at least two b-values. The patient selection process and the inclusion and exclusion criteria are depicted in **Figure 1**.

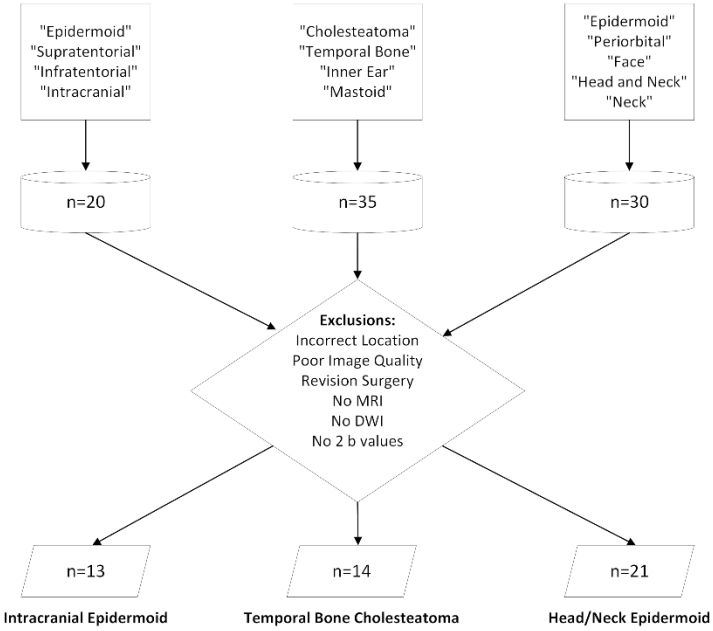

Figure 1. Study samples selection process.

Imaging data acquisition

The examinations were performed on a 1.5 or 3 Tesla magnet (Siemens Medical Solutions, Erlangen, Germany). Imaging was performed with a mixture of traditional single shot EPI (with parallel imaging and minimal time to echo) and also readout-segmented multishot EPI with parallel imaging and long variable echo-trains in order to decrease susceptibility and geometric distortion artifacts. Patients with inadequate imaging were excluded. ADC was measured using two b-values of 0 and 1000 s/mm2 for axial echoplanar DWI sequence and ranges for Time to Echo (TE) = 54 to 127 ms, Repetition Time (TR) = 3000 to 11000 ms, slice thickness = 2 to 5 mm, and interslice gap = 0 to 2.25 mm.

Image analysis

Lesions were assessed using DWI and manually segmented using a parametric software (pMRI) (https://www.parametricmri.com). Diffusivity metrics were calculated on a pixel-by-pixel basis. All imaging was retrospectively reviewed by a pediatric neuroradiologist with over ten years of experience. Normal tissues, such as brain, bone, CSF, skin, and subcutaneous tissue, were excluded from the regions of interest (ROI) by referencing T1-weighted images (T1WI) and T2-weighted images (T2WI). Care was taken not to place the region of interest in areas of susceptibility artifact. Similarly, the outer 2 mm of the lesion periphery, as well as the most cranial and caudal axial sections of the lesion, were excluded to prevent partial volume averaging.

DWI images were post-processed using pMRI. ROIs were placed over the lesion, thalamus, cerebellum, and cerebral white matter. Average ADC values and histogram metrics, including minimum, maximum, median, and skewness, were calculated by fitting the signal intensities at each pixel in the b=0 and b=1000 images to the equation S(b) = S0 * e-ADC*b, where b represents the b-value [s/mm²], S(b) represents the signal intensity when the b-value equals b, S_0 is the computed signal intensity at a b-value of 0, and ADC the apparent diffusion coefficient [10-6mm2/s]. A senior board-certified pediatric neuroradiologist reviewed the segmentation process and approved the results.

We used a second software for validation to ensure the accuracy of the diffusion analysis results obtained via pMRI. The software FireVoxel (FV) (http://www.firevoxel.com) was selected to recalculate the diffusion computation. To mitigate discrepancies arising from differences in ROI creation between the two software tools, we utilized the exact ROIs initially delineated in pMRI. Thus, all ROIs present in pMRI were exported as Neuroimaging Informatics Technology Initiative (NIfTI) files and subsequently imported into FV, ensuring that the ROIs in both software applications were fully aligned. **Figure 2** displays screenshots of both pMRI and FV, showing the same image series with their corresponding ROIs. Examples of the DWI and T2-weighted images of the three types of lesions are shown in **Supplementary Figure 1**. An example of region of interest placement for a temporal bone cholesteatoma is shown in **Supplementary Figure 2**.

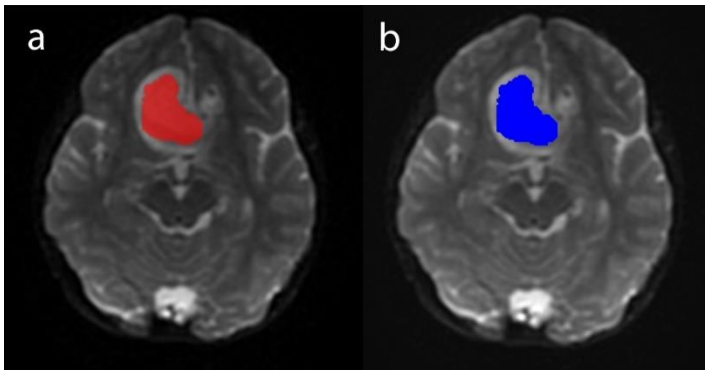

Figure 2. An example of a region of interest (ROI) used in pMRI (a) and FireVoxel (b) software to calculate the ADC values. The same ROI selection was used in both programs to ensure accurate and similar ADC values and to eliminate possible errors in multiple ROI Creation

Statistical Analysis

Statistical analysis was conducted using IBM SPSS Statistics for Windows (version 26.0; IBM Corp., Armonk, NY). Nominal data were presented as percentages, while quantitative data were represented as medians (range). The agreement between software calculations of ADC was assessed using the intraclass correlation coefficients (ICC) with a two-way random effects mode for absolute agreement among multiple measurements and also Bland-Altman analysis. Differences among the values and histogram features of the lesions and normal brain tissues were evaluated using the Wilcoxon rank-sum and Kruskal-Wallis tests. Statistical significance was defined as a p-value of less than 0.05.

RESULTS

Forty-eight patients were included in this study. Thirteen (27.1%) patients had IE, 14 (29.2%) had EC, and 21 (43.7%) had TBC. The mean age of the patients was 8.67 ± 5.30 years, and twenty-seven (56.3%) were female.

Each lesion ADC values were calculated using pMRI and the FireVoxel software. The calculated mean ADC values of the lesions were 1,118.52 ± 516.90 mm²/s for pMRI and 1,134.79 ± 504.88 mm²/s for FireVoxel, with an Intraclass Correlation Coefficient (ICC) of 0.997 (95% CI: 0.995 - 0.998). **Table 1** provides additional details for other histogram metrics and their respective ICCs. The Bland-Altman plot also demonstrates that the mean difference between the ADC values calculated by the two programs is just 19.23 mm²/s, with 45 out of 48 data points (93.75%) falling within the upper and lower limits of agreement (LoA) (**Figure 3**).

The median ADC values were 973.7x10-6 mm2/s for IE, 875.7x10-6 mm2/s for EC, and 933.2x10-6 mm2/s for TBC, respectively (Figure 4). As the Shapiro-Wilk test indicated that the distribution of median ADC values significantly deviates from the normal distribution ($p < 0.001$), the Kruskal-Wallis test was employed to compare the ADC values of IE, EC, and

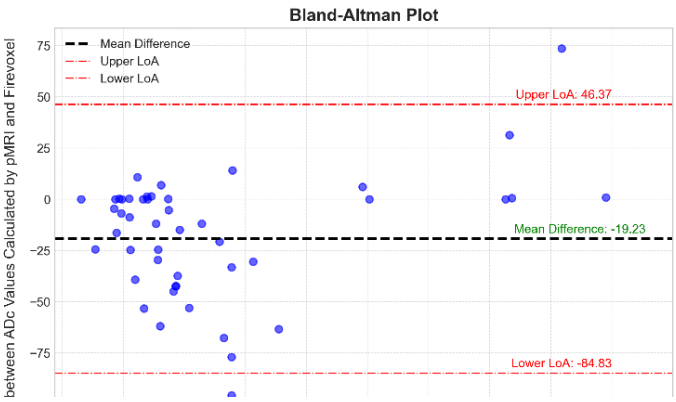

Figure 3 A Bland-altman plot comparing the ADC values between pMRI and FireVoxel. The mean difference in ADC values between the two programs is -19.23 x 10-3 mm2/s. The 95% limit of agreement is at +46.37 and -84.83 x 10-3 mm2/s. Except for three outliers, all scores fall within the 95% range and are distributed randomly and equally within the upper and lower range, showing good reliability between the two programs.

TBC. The results revealed no significant differences among the three groups (p = 0.265). The median ADC values of the thalamus, cerebellum, and white matter were 789x10-6 mm2/s, 730x10-6 mm2/s, and 802x10-6 mm2/s, respectively (**Figure 4**). When comparing the median ADC values of normal brain regions with those of all three different lesions using the Wilcoxon rank-sum test, the ADC values of the lesions were found to be significantly higher (933 vs. 766, x10-6 mm2/s, p < 0.0001). The median ADC of the lateral ventricular CSF was 3193x10-6 mm2/s and significantly higher than the various brain regions and three types of tissues analyzed (p<0.001). Subgroup analyses for each brain region and lesion type are presented in **Table 2.**

Table 1. Mean ADC values calculated by pMRI and FireVoxel and their degree of agreement.

	pMRI	Firevoxel	ICC
Mean			
IE	1116.49±279.6	1145.52±301.01	0.989 (0.960-997)
EC	918.85±194.93	942.89±200.64	0.976 (.924-992)
TBC	1252.89±713.73	1256.07±690.79	0.999 (0.997-1.000)
All	1118.52±516.90	1134.79±504.88	0.997 (0.995-.998)
Thalamus	794.77±80.36	-	-
Cerebellum	743.31±50.20	-	-
White Matter	794.27±89.04	-	-
Median			
IE	1114.94±316.79	1140.22±336.09	0.996 (0.979-0.998)
EC	921.44±196.32	956.50±213.52	0.987 (0.835-0.994)
TBC	1257.79±728.50	1262.73±714.60	1.000 (0.999-1.000)
All	1121±531.36	1140.23±524.89	0.999 (0.996-0.999)
Thalamus	794.97±81.54	-	-
Cerebellum	732.22±48.99	-	-
White Matter	791.59±88.95	-	-
Minimum			
IE	701.45±176.90	666.58±213.87	0.949 (0.835-0.984)
EC	590.49±590.49	594.39±289.36	0.998 (0.994-0.999)
TBC	784.36±584.16	799.72±598.85	0.998 (0.995-0.999)
All	705±426	703±442	0.995 (0.992-0.997)
Thalamus	488±184.60	-	-
Cerebellum	504.51±116.45	-	-
White Matter	522.51±150.41	-	-
Maximum			
IE	1968.01±940.52	2355.06±1906.38	0.787 (0.334-0.934)
EC	1266.73±414.23	1244.46±288.98	0.897 (0.676-0.967)
TBC	1756.67±866.75	1757.27±822.05	0.995 (0.988-0.998)
All	1671±818	1769±1189	0.878 (0.784-0.932)
Thalamus	1118.58±244.78	-	-
Cerebellum	1167.75±288.11	-	-
White Matter	1115.89±145.48	-	-
Skewness			
IE	0.76±1.10	0.93±1.23	0.914 (0.728-0.973)
EC	-0.07±0.71	-0.17±0.57	0.881 (0.640-.0962)
TBC	0.09±0.80	0.08±0.81	0.995 (0.988-0.998)
All	0.22±0.91	0.24±0.97	0.949 (0.909-0.971)
Thalamus	0.004±0.28	-	-
Cerebellum	0.87±0.59	-	-
White Matter	0.17±0.38	-	-

Table 2 Comparison of median ADC values of Lesions and Normal Brain Parts using Wilcoxon rank-sum test

Lesion ADC Values \ Brain ADC Values		Thalamus	Cerebellum	White Matter	All Normal Brain parts
		789	730	802	766
IE	973	<0.001	<0.001	<0.001	<0.001
TBC	933	0.008	<0.001	0.003	<0.001
EC	875	0.025	<0.001	0.02	0.002
All Lesions	933	<0.001	<0.001	<0.001	<0.001

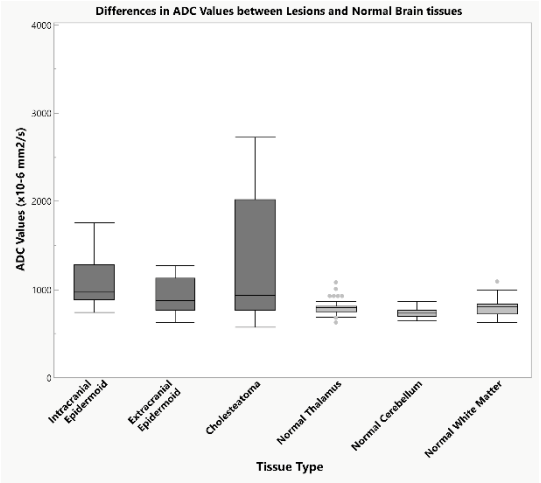

Figure 4. Box plot of the median ADC value of lesions (intracranial and extracranial epidermoids, cholesteatoma) in comparison to the ADC values of normal brain area (Normal thalamus, cerebellum, and white matter). Comparison between the ADC values of each lesion showed no statistically significant differences between the lesions ($p = 0.265$). Comparison between the ADC values of each pathology to each normal reference area and between the values of all pathologies to all normal control areas are all found to have a statistically significant difference ($p < 0.001$).

DISCUSSION

Major advancements in neuroimaging, particularly with DWI and ADC, have been made since the foundational work of Le Bihan et al.[23]. ADC plays a vital role in measuring water diffusion in the brain, which is critical for evaluating microstructure and identifying characteristics of gray and white matter and CSF [24]. ADC values are highest in CSF, reflecting its free-flowing nature; they are higher in the cerebral cortex than in white matter due to higher water and blood flow and intermediate in the basal ganglia and thalamus, indicating their unique microstructures [25]. For perspective, free water ADC in an aqueous solution at 37.5°C is approximately 3.0 x 10-3 mm²/sec but 2 to 10 times lower in the brain parenchyma [23]. This difference leads to consistently lower diffusivity in normal brain parenchyma compared to CSF and CSF-filled structures like arachnoid cysts.

Epidermoids or epidermoid cysts are ectodermal-derived congenital or acquired encapsulated lesions or nodules lined by stratified squamous epithelium and filled with luminal keratin. Similarly, congenital or acquired cholesteatomas show bland, keratinizing, stratified squamous epithelium and anucleate squares with keratinous debris. The lining and composition of these lesions are used for histopathological differentiation. The keratin contents often define the imaging characteristics and distinguish them from the more fluid contents of other cysts and cyst-like lesions [12,18-19,26]. In 1990, Tsuruda et al. first demonstrated that ADC aids in diagnosing 'cystic-appearing' extra-axial brain lesions 12. IEs, which are 'cystic appearing' lesions but with more solid content, were found to have restricted diffusion relative to CSF but not when compared to normal parenchyma. Their study revealed that the ADC of arachnoid cysts approximates stationary water, whereas the ADC of IEs is similar to brain parenchyma [12]. Contrary to these initial descriptions, a major portion of the imaging literature, including book chapters and radiology reports, continues to describe IEs, TBCs, and ECs as exhibiting diffusion restriction without specifying the comparator tissue and which leads to erroneous conclusions and issues with interpretation. Numerous research studies show that IEs demonstrate restricted diffusion [18,19]. However, a few studies have otherwise suggested the absence of such diffusion restriction in IEs [26,27]. For TBCs, most papers report that they exhibit diffusion restriction [20,21]. Multiple studies examining the DWI characteristics of ECs describe these lesions as also exhibiting restricted diffusion [6,22].

IEs, TBCs, and ECs are recognized for their high DWI signal, a key distinguishing characteristic, though the reason behind this in these conditions is still debated in some papers [28]. In medical imaging, DWI hyperintensity can result from a combination of restricted water movement and the T2 effects (T2 shine-through) [8,29]. Accordingly, the qualitative evaluation of ADC map images plays a crucial role in differentiating these causes [29]. Quantitative ADC values offer a more objective assessment of water diffusion in brain lesions or parenchyma [30]. Higher ADC values indicate greater water molecule diffusivity, typical of CSF and vasogenic edema, while lower ADC values suggest restricted water movement, as in ischemic cells or densely cellular tumors [31].

In our study, all three entities showed higher ADC values than the white matter, thalamus, and cerebellum, confirming that their hyperintense DWI signal is not due to restricted diffusion relative to the normal brain. Our findings also demonstrated that the ADC values of all three conditions are comparable, underscoring their shared origin and similar characteristics. The term 'restricted or reduced diffusion' should be relative and needs comparison with a reference structure. For instance, ADC values of CSF are higher than those of any other brain tissue, as all tissues have some degree of diffusion restriction compared to free water and CSF. Consequently, all brain regions will display restricted diffusion if the reference point is water or CSF. Preferably, when evaluating ADC maps, the focus should be identifying diffusion restriction or reduced diffusivity relative to neighboring tissues. Ideally, the ADC value within the lesion should be statistically significantly lower than that of the surrounding tissues and visually distinguishable.

In this study, as all lesions were confined to the head and neck region, we used the cerebellum, white matter, and thalamus as reference points to compare with ADC values of IE, TBC, and EC. For these lesions to be classified as having restricted diffusion, their ADC values should have been lower than those in other brain parts. Nevertheless, our findings revealed that the ADC values of these lesions were, in fact, statistically higher than those of the brain. We utilized pMRI and histogram metrics of IE, TBC, and EC to evaluate the ADC values. To ensure the precision of this software, we also used another software, FireVoxel, to calculate the ADC values of these lesions using the same ROIs as in the initial software calculation. Based on our findings, the calculated ADC values from pMRI and Firevoxel are similar. When comparing the means of ADC values, the Intraclass Correlation Coefficient (ICC) was 0.997. For the ADC medians, the ICC was even higher at 0.999. The lowest ICC value between these two applications, 0.878, was found when we compared the maximum ADC values of these lesions. This suggests a slightly higher heterogeneity and lower degree of agreement when analyzing lesions with high ADC values.

Moreover, the Bland-Altman plot comparing the ADC values between the two software applications demonstrates good agreement and

consistency in the measurements. The mean difference of measurements between these two applications was only 19.23, indicating that, on average, the ADC values obtained from both software are highly similar. Additionally, the upper and lower limits of agreement (LoA), typically set at ±1.96 standard deviations of the differences (ranging from -84.83 to 46.37), encompass the majority of the data points (93.75%). This further confirms the strong concordance between the two methods.

In IE, the hyperintensity observed in DWI was initially considered to result from restricted water movement due to the histological arrangement of concentric keratin filaments [28]. However, some studies have demonstrated that IE may exhibit ADC value similar in appearance to the surrounding brain parenchyma 12,13. Most of the studies that measured the ADC values of IE had small sample sizes. Chen et al. reported 1.197 x 10-3 mm2/s in 8 IE patients 14, Annet et al. reported 1.070 x 10-3 mm2/s in 6 patients 15; and Hakyemez et al. 1.157 x 10-3 mm2/s in 15 IE patients 16. Our results align with some of these previous studies, with a mean ADC value of 1.116 x 10-3 mm2/s obtained from the DWI of pediatric 13 IEC patients. In a study involving 15 patients with IEs, Hakyemez et al. discovered that the ADC values of ECs were notably lower than CSF yet higher than deep white matter. They also observed that ECs showed similar intensity in exponential DWI to brain parenchyma. This finding suggests that the hyperintensity seen in trace images of ECs is primarily due to an enhanced T2 effect in the tissue rather than a decrease in ADC values 16.

ECs are typically found subcutaneously [22]. However, studies using MRI to evaluate these lesions are scarce since most are diagnosed clinically [22]. Imaging evaluations of these lesions in the head and neck region are even rarer. In a previous study, the ADC value of subcutaneous epidermal cysts has been documented to be 0.81 x 10-3 mm2/s from a sample of 14 patients [32]. Our mean ADC value of 0.918 x 10-3 mm2/s is slightly higher. Suzuki et al. measured epidermoid cysts located intracranially and subcutaneously and found a statistically significant difference, with intracranial cysts exhibiting a much higher ADC value [32]. In contrast, our results did not show a statistical difference between IEs, TBCs, and ECs. However, the sample size in these studies is limited, and further research is needed to clarify the true cause of this discrepancy.

Like epidermoids, cholesteatoma is a benign lesion caused by the excessive growth of keratinizing squamous epithelium [33]. While high-resolution CT is the primary imaging modality for diagnosing cholesteatoma, the characteristic DWI hyperintensity of TBC has been shown to enhance the accurate diagnosis of these lesions [20]. This feature has also been used to rule out recurrence during follow-up [34]. The DWI and ADC maps of these lesions is often compared to that of the brain since it is the often the main tissue with adequate signal for comparison on trace DWI images. Only one previous study by Thiriat et al. in 2009 measured ADC value quantitatively in 9 patients with cholesteatoma, with a mean value of 0.903 x 10-3 mm2/s, different than the mean ADC value of an abscess 0.415 x 10-3 mm2/s [35]. These findings generally align with our study's mean ADC value of 1.252 x 10-3 mm2/s in 21 TBC patients, suggesting restricted diffusion (relative to brain) is not the cause of lesion hyperintensity on DWI.

This paper is the first to address these three types of lesions comprehensively in a pediatric cohort by ADC histogram analysis with rigorous inclusion and exclusion criteria. Its strengths include strict inclusion and exclusion criteria, by including pathology-proven cases only, using two distinct software to calculate ADC to ensure accuracy, and double-checking ROIs. A potential limitation of our retrospective study is the that the regions of interest may overlook microscopic pockets of CSF, calcification, or blood products in the lesions.

CONCLUSIONS

The ADC values for IEs, TBCs, and ECs are higher than those of normal brain tissues, including the cerebellum, white matter, and thalamus. Consequently, these entities should not be classified as having restricted diffusion or reduced diffusivity without designating a comparator tissue or using the brain as a comparator, despite the literature and this study suggesting otherwise. The hyperintensity observed on DWI is likely relatively more attributable to T2 shine-through effect. If the comparison is explicitly made to CSF, then using the term restricted diffusion is accurate. While diffusion imaging remains crucial for visualizing these anomalies, accurate medical terminology should be used in reports to describe these findings appropriately. Further investigations are essential to ascertain whether similar lesions in other body regions also have a relatively smaller magnitude of diffusion restriction and whether distinguishing between dermoids and epidermoids using quantitative assessments of ADC values is possible.

REFERENCES

1. Pop MM, Bouros D, Klimko A, Florian IA, Florian IS. Intracranial epidermoid cysts: benign entities with malignant behavior: experience with 36 cases. *Sci Rep*. 2023;13(1):6474. doi:10.1038/s41598-023-33617-x
2. Davidoss N, Ha J, Banga R, Rajan G. Delayed Presentation of a Congenital Cholesteatoma in a 64-year-old Man: Case Report and Review of the Literature. *J Neurol Surg Rep*. 2014;75(1):e113-6. doi:10.1055/s-0034-1376200
3. Santos HB, Rolim LS, Barros CC, Cavalcante IL, Freitas RD, Souza LB. Dermoid and epidermoid cysts of the oral cavity: a 48-year retrospective study with focus on clinical and morphological features and review of main topics. *Med Oral Patol Oral Cir Bucal*. 2020;25(3):e364-e369. doi:10.4317/medoral.23388
4. Felici F, Scemama U, Bendahan D, et al. Improved Assessment of Middle Ear Recurrent Cholesteatomas Using a Fusion of Conventional CT and Non-EPI-DWI MRI. *AJNR Am J Neuroradiol*. 2019;40(9):1546-1551. doi:10.3174/ajnr.A6141
5. Chowdhury FH, Haque MR, Sarker MH. Intracranial epidermoid tumor; microneurosurgical management: An experience of 23 cases. *Asian J Neurosurg*. 2013;8(1):21-28. doi:10.4103/1793-5482.110276
6. Pupić-Bakrač J, Pupić-Bakrač A, Bačić I, Kolega MŠ, Skitarelić N. Epidermoid and dermoid cysts of the head and neck. *J Craniofac Surg*. 2021;32(1):e25-e27. doi:10.1097/SCS.0000000000006834
7. Bazzi K, Wong E, Jufas N, Patel N. Diffusion-weighted magnetic resonance imaging in the detection of residual and recurrent cholesteatoma in children: A systematic review and meta-analysis. *Int J Pediatr Otorhinolaryngol*. 2019;118:90-96. doi:10.1016/j.ijporl.2018.12.031
8. Burdette JH, Elster AD, Ricci PE. Acute cerebral infarction: quantification of spin-density and T2 shine-through phenomena on diffusion-weighted

MR images. *Radiology*. 1999;212(2):333-339. doi:10.1148/radiology.212.2.r99au36333
9. Herneth AM, Guccione S, Bednarski M. Apparent diffusion coefficient: a quantitative parameter for in vivo tumor characterization. *Eur J Radiol*. 2003;45(3):208-213. doi:10.1016/s0720-048x(02)00310-8
10. Humphries PD, Sebire NJ, Siegel MJ, Olsen ØE. Tumors in pediatric patients at diffusion-weighted MR imaging: apparent diffusion coefficient and tumor cellularity. *Radiology*. 2007;245(3):848-854. doi:10.1148/radiol.2452061535
11. Hiwatashi A, Kinoshita T, Moritani T, et al. Hypointensity on diffusion-weighted MRI of the brain related to T2 shortening and susceptibility effects. *AJR Am J Roentgenol*. 2003;181(6):1705-1709. doi:10.2214/ajr.181.6.1811705
12. Tsuruda JS, Chew WM, Moseley ME, Norman D. Diffusion-weighted MR imaging of the brain: value of differentiating between extraaxial cysts and epidermoid tumors. *AJR Am J Roentgenol*. 1990;155(5):1059-1065; discussion 1066. doi:10.2214/ajr.155.5.2120936
13. Maeda M, Kawamura Y, Tamagawa Y, et al. Intravoxel incoherent motion (IVIM) MRI in intracranial, extraaxial tumors and cysts. *J Comput Assist Tomogr*. 1992;16(4):514-518. doi:10.1097/00004728-199207000-00003
14. Chen S, Ikawa F, Kurisu K, Arita K, Takaba J, Kanou Y. Quantitative MR evaluation of intracranial epidermoid tumors by fast fluid-attenuated inversion recovery imaging and echo-planar diffusion-weighted imaging. *AJNR Am J Neuroradiol*. 2001;22(6):1089-1096.
15. Annet L, Duprez T, Grandin C, Dooms G, Collard A, Cosnard G. Apparent diffusion coefficient measurements within intracranial epidermoid cysts in six patients. *Neuroradiology*. 2002;44(4):326-328. doi:10.1007/s00234-001-0726-2
16. Hakyemez B, Aksoy U, Yildiz H, Ergin N. Intracranial epidermoid cysts: diffusion-weighted, FLAIR and conventional MR findings. *Eur J Radiol*. 2005;54(2):214-220. doi:10.1016/j.ejrad.2004.06.018
17. Fitzek C, Mewes T, Fitzek S, Mentzel H-J, Hunsche S, Stoeter P. Diffusion-weighted MRI of cholesteatomas of the petrous bone. *J Magn Reson Imaging*. 2002;15(6):636-641. doi:10.1002/jmri.10118
18. Kumar A, Maurya VP, Kanjilal S, et al. Clinicoradiological features and treatment outcome of supratentorial intraparenchymal epidermoid cyst: A report of five cases and literature review. *J Neurosci Rural Pract*. 2021;12(3):571-580. doi:10.1055/s-0041-1730125
19. Bergui M, Zhong J, Bradac GB, Sales S. Diffusion-weighted images of intracranial cyst-like lesions. *Neuroradiology*. 2001;43(10):824-829. doi:10.1007/s002340100595
20. Corrales CE, Blevins NH. Imaging for evaluation of cholesteatoma: current concepts and future directions. *Curr Opin Otolaryngol Head Neck Surg*. 2013;21(5):461-467. doi:10.1097/MOO.0b013e328364b473
21. Jindal M, Riskalla A, Jiang D, Connor S, O'Connor AF. A systematic review of diffusion-weighted magnetic resonance imaging in the assessment of postoperative cholesteatoma. *Otol Neurotol*. 2011;32(8):1243-1249. doi:10.1097/MAO.0b013e31822e938d
22. Hoang VT, Trinh CT, Nguyen CH, Chansomphou V, Chansomphou V, Tran TTT. Overview of epidermoid cyst. *European J Radiol Open*. 2019;6:291-301. doi:10.1016/j.ejro.2019.08.003
23. Le Bihan D. Apparent diffusion coefficient and beyond: what diffusion MR imaging can tell us about tissue structure. *Radiology*. 2013;268(2):318-322. doi:10.1148/radiol.13130420
24. Palombo M, Shemesh N, Ronen I, Valette J. Insights into brain microstructure from in vivo DW-MRS. *Neuroimage*. 2018;182:97-116. doi:10.1016/j.neuroimage.2017.11.028
25. Helenius J, Soinne L, Perkiö J, et al. Diffusion-weighted MR imaging in normal human brains in various age groups. *AJNR Am J Neuroradiol*. 2002;23(2):194-199.
26. Lian K, Schwartz ML, Bilbao J, Perry J, Aviv RI, Symons SP. Rare frontal lobe intraparenchymal epidermoid cyst with atypical imaging. *J Clin Neurosci*. 2012;19(8):1185-1187. doi:10.1016/j.jocn.2011.11.003
27. Puranik A, Sankhe S, Goel N, Mahore A. Cerebral shading sign in a giant intraparenchymal white epidermoid. *Neurol India*. 2012;60(2):265-266. doi:10.4103/0028-3886.96439
28. Andica C, Hori M, Kamiya K, et al. Spatial Restriction within Intracranial Epidermoid Cysts Observed Using Short Diffusion-time Diffusion-weighted Imaging. *Magn Reson Med Sci*. 2018;17(3):269-272. doi:10.2463/mrms.cr.2017-0111
29. Provenzale JM, Engelter ST, Petrella JR, Smith JS, MacFall JR. Use of MR exponential diffusion-weighted images to eradicate T2 "shine-through" effect. *AJR Am J Roentgenol*. 1999;172(2):537-539. doi:10.2214/ajr.172.2.9930819
30. Huisman TAGM. Diffusion-weighted and diffusion tensor imaging of the brain, made easy. *Cancer Imaging*. 2010;10 Spec no A:S163-71. doi:10.1102/1470-7330.2010.9023
31. Castillo M, Mukherji SK. Diffusion-weighted imaging in the evaluation of intracranial lesions. *Seminars in Ultrasound, CT and MRI*. 2000;21(6):405-416. doi:10.1016/S0887-2171(00)90033-7
32. Suzuki C, Maeda M, Matsumine A, et al. Apparent diffusion coefficient of subcutaneous epidermal cysts in the head and neck comparison with intracranial epidermoid cysts. *Acad Radiol*. 2007;14(9):1020-1028. doi:10.1016/j.acra.2007.05.014
33. Pachpande TG, Singh CV. Diagnosis and treatment modalities of cholesteatomas: A review. *Cureus*. 2022;14(11):e31153. doi:10.7759/cureus.31153
34. Dubrulle F, Souillard R, Chechin D, Vaneecloo FM, Desaulty A, Vincent C. Diffusion-weighted MR imaging sequence in the detection of postoperative recurrent cholesteatoma. *Radiology*. 2006;238(2):604-610. doi:10.1148/radiol.2381041649
35. Thiriat S, Riehm S, Kremer S, Martin E, Veillon F. Apparent diffusion coefficient values of middle ear cholesteatoma differ from abscess and cholesteatoma admixed infection. *AJNR Am J Neuroradiol*. 2009;30(6):1123-1126. doi:10.3174/ajnr.A1473

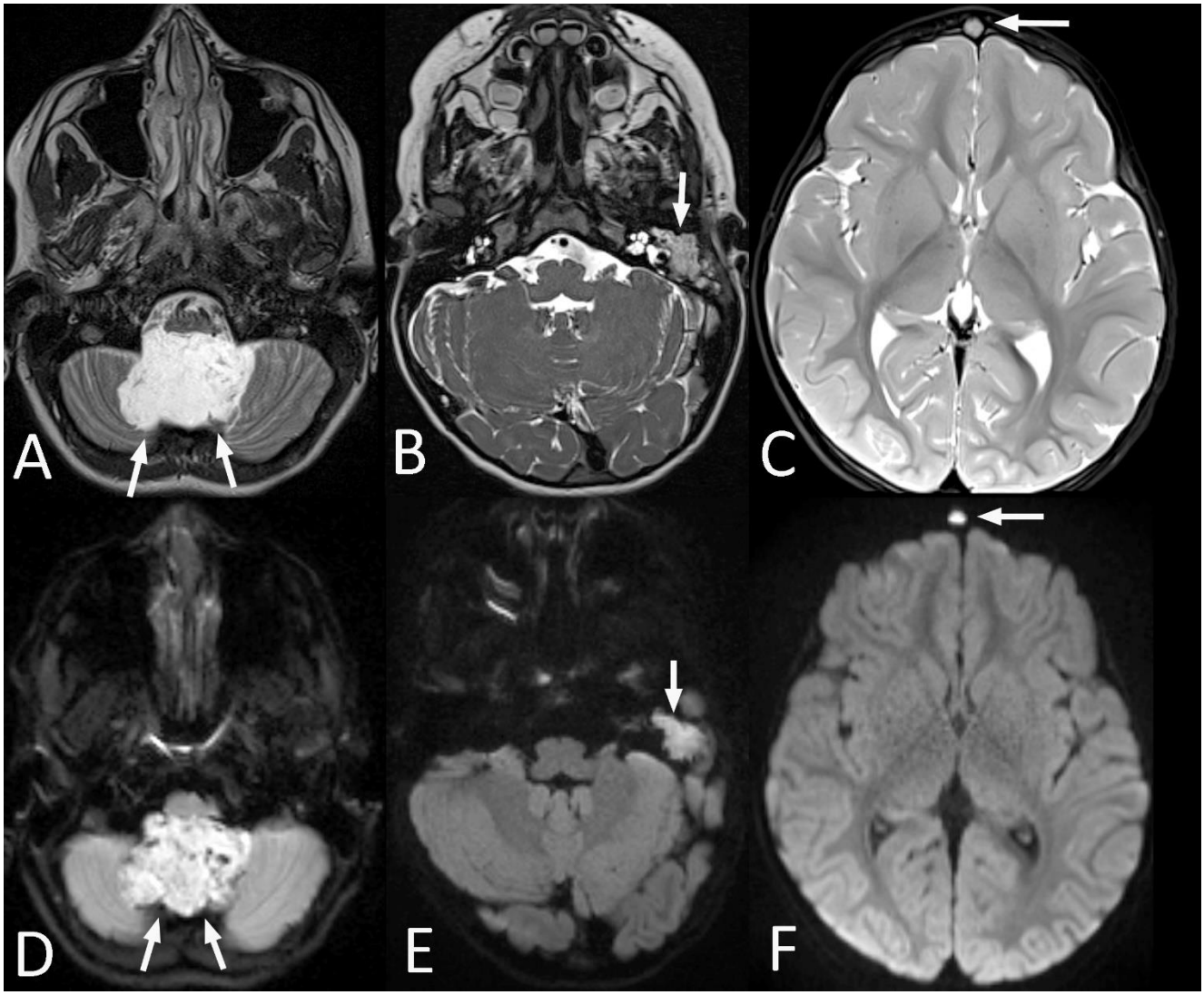

Supplementary Figure 1. Axial T2-weighted imaging (top row) and DWI trace images (bottom row) images showing an intracranial epidermoid (A, D), temporal bone cholesteatoma (B,E), and head and neck (glabellar) epidermoid (C, F) (arrows).

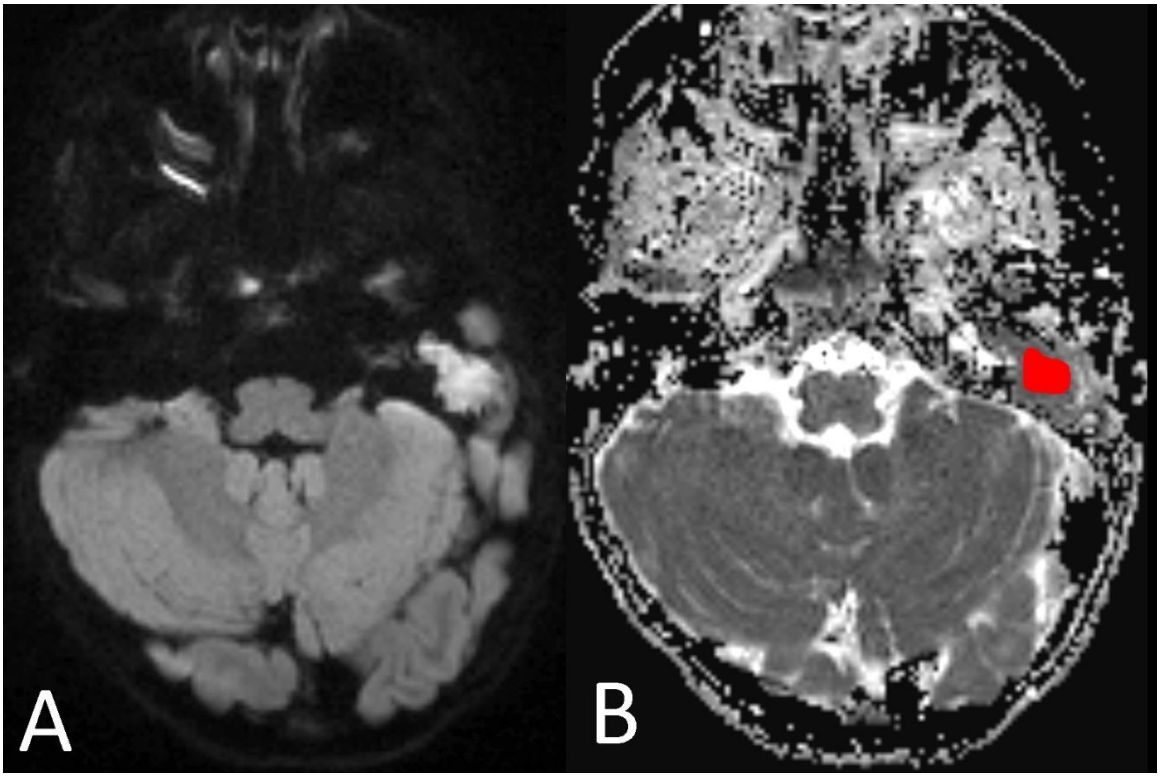

Supplementary Figure 2. Sample axial DWI (A) and ADC map (B) demonstrating placement of the region for ADC analysis.